

## Accepted Manuscript

Synthesis of Graphene Quantum Dots Stabilized Bimetallic AgRh Nanoparticles and Their Applications

Ning Li, Weifeng Chen, Jialu Shen, Shaona Chen, Xiang Liu

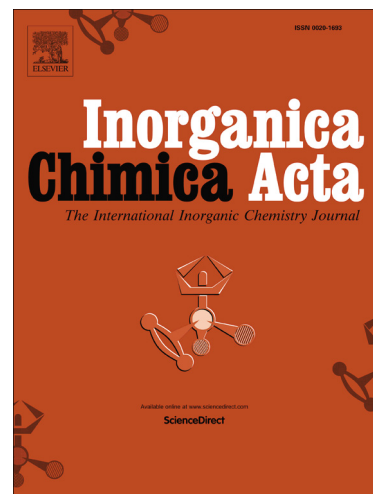
PII: S0020-1693(19)30761-3  
DOI: <https://doi.org/10.1016/j.ica.2019.119031>  
Article Number: 119031  
Reference: ICA 119031

To appear in: *Inorganica Chimica Acta*

Received Date: 24 May 2019  
Revised Date: 12 July 2019  
Accepted Date: 20 July 2019

Please cite this article as: N. Li, W. Chen, J. Shen, S. Chen, X. Liu, Synthesis of Graphene Quantum Dots Stabilized Bimetallic AgRh Nanoparticles and Their Applications, *Inorganica Chimica Acta* (2019), doi: <https://doi.org/10.1016/j.ica.2019.119031>

This is a PDF file of an unedited manuscript that has been accepted for publication. As a service to our customers we are providing this early version of the manuscript. The manuscript will undergo copyediting, typesetting, and review of the resulting proof before it is published in its final form. Please note that during the production process errors may be discovered which could affect the content, and all legal disclaimers that apply to the journal pertain.



## Synthesis of Graphene Quantum Dots Stabilized Bimetallic AgRh Nanoparticles and Their Applications

Ning Li,<sup>a#</sup> Weifeng Chen,<sup>a#</sup> Jialu Shen,<sup>a</sup> Shaona Chen,<sup>a</sup> and Xiang Liu<sup>a,b\*</sup>

<sup>a</sup>College of Materials and Chemical Engineering, Key Laboratory of Inorganic Nonmetallic Crystalline and Energy Conversion Materials, China Three Gorges University, Yichang, Hubei 443002, China. Email: [xiang.liu@ctgu.edu.cn](mailto:xiang.liu@ctgu.edu.cn)

<sup>b</sup>Material Analysis and Testing Center, China Three Gorges University, Yichang, Hubei 443002, China.

<sup>#</sup>These authors are contributed equally to this work and should be considered as co-first authors

### Abstract

The design and synthesis of highly efficient and ultrafine bimetallic nanoparticles catalysts is challenging. Here we report the synthesis of AgRh bimetallic nanoparticles (AgRh BNPs) stabilized by graphene quantum dots (GQDs) and their exceptional catalytic activities in the reduction of 4-nitrophenol, 2,4-dinitrophenol and 4-nitrobenzene diazonium tetrafluoroborate and generation of hydroxyl radicals. Construction of AgRh BNPs nanocomposites is accomplished by mixing of GQDs and sodium borohydride, followed by the addition of simple commercial Ag and Rh salt at 0°C in water. Among them, AgRh BNPs 4 exhibits excellent catalytic performance owing to a positive synergistic effects between the Ag and Rh atoms on GQDs, and its catalytic activity is better than those of both monometallic counterparts.

## Introduction

In the last few decades, bimetallic nanoparticle (BNPs) with novel compositions and well-defined structures are of particular current interest due to their composition-dependent electronic, optical and catalytic properties.<sup>[1]</sup> They have been widely used as efficient heterogeneous or homogeneous catalysts for a broad range of inorganic and organic reactions,<sup>[2]</sup> owing to the synergistic effects between different metal atoms of BNPs often result in remarkable enhancement of the overall catalytic activity and selectivity by restructuring the average binding energy of the surface of BNPs, compared with monometallic nanoparticles.<sup>[3]</sup> As a result, plenty of cost-effective BNPs catalysts have been developed by dilution of scarce and noble metals using comparatively earth-abundant metals. AgRh bimetallic nanoparticles has generated enormous excitement because of its wide applications in the hydrogen absorption,<sup>[4]</sup> catalysis<sup>[5]</sup> and oxynitride decomposition.<sup>[6]</sup> The AgRh BNPs system has thus been utilized as an effective method to further improve catalytic activity and selectivity and to reduce the required amount of Rh by alloying with much cheaper and more abundant Ag, since Rh is extremely scarce and expensive. Although Ag and Rh are immiscible even at 2000 °C in bulk form, this problem has been recently solved by reducing the NPs size to a very few nm.<sup>[7]</sup> However, the physical and chemical behavior of AgRh BNPs have been less investigated than other BNPs, therefore, an efficient and simple way to construct AgRh BNPs is still necessary.

Graphene quantum dots (GQDs) have attracted considerable attention from researchers due to their low toxicity, biocompatibility and chemical inertness.<sup>[8]</sup> GQDs, consisting of ultrasmall fragments of graphene nanosheets, have the excellent chemical and physical properties of graphene, including high surface area, surface groups and better surface grafting using  $\pi$ - $\pi$  conjugation. Therefore, they have been successfully used as efficient catalyst supports for stabilizing transition metal nanoparticles (TMNPs). For example, AuNPs on GQDs for electrochemical detection of  $\text{H}_2\text{O}_2$  in biological environments,<sup>[9]</sup> for *S. aureus* specific gene detection<sup>[10]</sup> and for  $\text{Pb}^{2+}$  detection.<sup>[11]</sup> Our laboratory has long term interest in the synthesis of TMNPs and their application.<sup>[12]</sup> Hence, in this work, we first report the synthesis of various graphene quantum dots stabilized AgRh bimetallic nanoparticles and their exceptional catalytic activity in the reduction of 4-nitrophenol, 2,4-dinitrophenol and 4-nitrobenzene diazonium

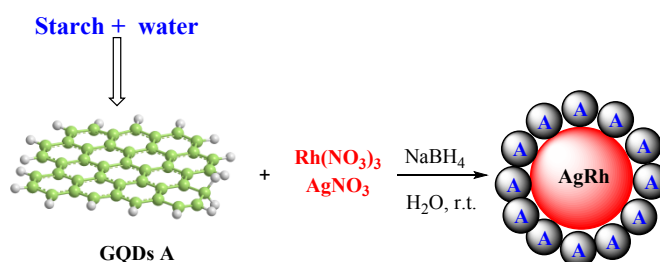


**Figure 1.** The synthesis of AgRh BNPs

tetrafluoroborate and generation of hydroxyl radicals. In our study, we used our previously reported GQDs A (**Figure 1**) with a narrow size distribution range from 2.25 to 3.50 nm as the model system for the AgRh BNPs supports.<sup>[13]</sup> GQDs A were made from only natural polymer starch and water, and have uniform structure. In addition, A is highly soluble in water, allowing for stabilizing AgRh BNPs to be conducted in water with great stability. GQDs plays a decisive role on stabilizing the nanoparticles in a controlled fashion to prevent the aggregation. Construction of the AgRh BNPs has been conducted here by direct coordination of Ag(I) and Rh(III) ions onto GQDs followed by NaBH<sub>4</sub> reduction in water. The alloyed nano-structure with optimized ratio 1:1 of Rh : Ag compositions is significantly more active as catalysts than Rh and Ag itself in the reduction of 4-nitrophenol, 2,4-dinitrophenol and 4-nitrobenzene diazonium tetrafluoroborate and generation of hydroxyl radicals.

## Experimental

### Chemicals and reagents

All commercial materials were used without further purification, unless indicated. The deionized water was prepared in the laboratory. The starch, AgNO<sub>3</sub>, Rh(NO<sub>3</sub>)<sub>3</sub>, 4-nitrophenol, 2,4-diaminophenol, 4-aminobenzene diazonium tetrafluoroborate, H<sub>2</sub>O<sub>2</sub> (w%, 30%), methylene blue and NaBH<sub>4</sub> were purchased from Aladdin Reagent Co., Ltd. (Shanghai, China, <http://www.aladdin-e.com/>).

### Instruments

UV-Vis absorption spectra were recorded on a UV1900 spectrophotometer (Shimadzu, China) with a 1 cm quartz cell. Transmission electron microscopy (TEM) measurements were performed on a TECNAI F-20 electron microscope (JEOL 2100F, Netherlands) at an accelerating voltage of 200 kV. Surface analysis by XPS was performed in a Thermo SCIENTIFIC ESCALAB 250Xi (ThermoFischer, USA) system spectrometer in an ultra-high vacuum (UHV) chamber.

### Preparation of the GQDs

GQDs were synthesized from only commercial natural polymer starch and water using our previously reported method.<sup>[13]</sup> The starch of 0.3g was firstly dispersed in 25 mL deionized water and stirred at 60°C for 15 min. After it is dissolved, the solution was immediately poured into a 100 mL Teflon lined stainless autoclave, which was then heated in an oven at 180 °C for 8 h. Then, the autoclave was taken out to be cooled freely. The final brown product was transferred into centrifugal tubes, and centrifuged at 10000 r/min for 30 min to separate out the precipitate. The pale yellow liquid which was obtained finally was the solution of graphene quantum dots (GQDs):

0.31 g/L.

#### The preparation of AgRh BNPs 4 as a general procedure

First, 1 mL(0.31 g/L) GQDs are dissolved in 2 mL of deionized water in a Schlenk flask, and the solution is stirred for 10 mins at 0 °C. Then a colorless solution of NaBH<sub>4</sub> (5 ×10<sup>-3</sup> mmol in 1 mL water) is added to the solution of GQDs. And the solution is stirred for 30 mins. A 1-mL aqueous solution containing 1.25×10<sup>-4</sup> mmol AgNO<sub>3</sub> and 1.25×10<sup>-4</sup> mmol RhNO<sub>3</sub> is added dropwise, provoking a color change to brownish yellow (**Figure S4**) due to the reduction of the cation to the zero-valent metal and formation of AgRh BNPs 4. The 4 were kept in aqueous solution for characterization and their used as the catalysts. AgRh BNPs 3 (**Figure S3**) and 5 (**Figure S5**) were synthesized in the same method.

#### Catalysis of 4-nitrophenol reduction

An aqueous solution (2.5 mL) containing 4-nitrophenol (0.09 mmol) and NaBH<sub>4</sub> (9 mmol) is prepared in a standard quartz cuvette (3 mL, path length: 1 cm). The TMNPs catalyst (5 mol%) is injected into this solution, and the reaction progress is detected by UV-vis. spectroscopic analysis every min at 22 °C. (Figure S6-S19)

#### Generation of Hydroxyl Radicals

An aqueous solution containing 3 mL of AgNPs (1.5×10<sup>-4</sup> mmol) and methylene blue (3.375×10<sup>-5</sup> mmol) is prepared in a standard quartz cuvette (3 mL, path length: 1 cm). The H<sub>2</sub>O<sub>2</sub> (0.1 eq -10 eq) is injected into this solution, and the reaction progress is detected by UV-vis. spectroscopic analysis every min at 22 °C. (Figure S20-S27)

### Results and Discussion

#### Synthesis of the AgNPs, RhNPs and AgRh BNPs

First, as a comparative experiment, Ag and Rh monometallic nanoparticles (**1** and **2**) were conducted by adding simple commercial silver nitrate and rhodium nitrate into a solution of as-synthesized GQDs and sodium borohydride at 0 °C, respectively. A color change to orange (AgNPs) due to the reduction of the cation to the zero-valent metal and formation of the AgNPs (**Figure 1**). The characteristic peak at 400 nm of AgNP, with a size of 14.65 nm, has also been observed in UV-vis spectra (**Table 1 and Figure 2a**), while RhNPs (2.14 nm) appear by TEM (vide infra) to be too small to be plasmonic (**Figure 2b**). Then, we further synthesized AgRh BNPs **3-5** by dilution of Rh with Ag that altered the Ag to Rh molar ratios, for further increasing the catalytic efficiency and selectivity and to reduce the required amount of Rh.

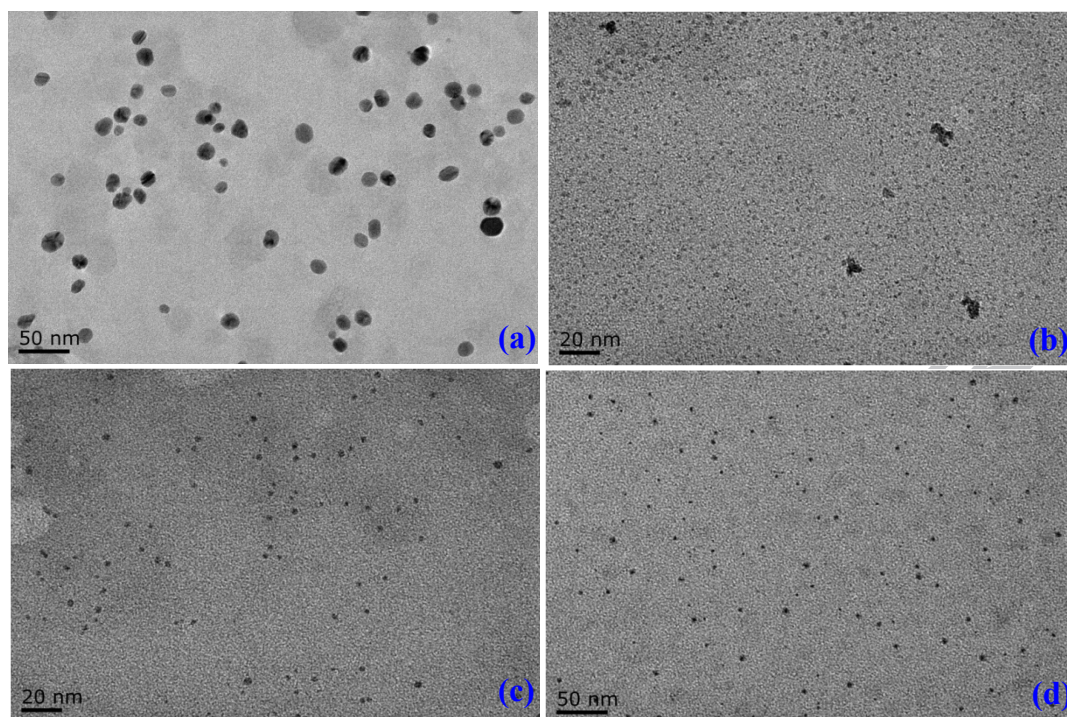


**Figure 2.** TEM images of AgNPs (a), Rh NPs(b), AgRh<sub>2</sub> NPs (c) and Ag<sub>2</sub>Rh NPs (d)

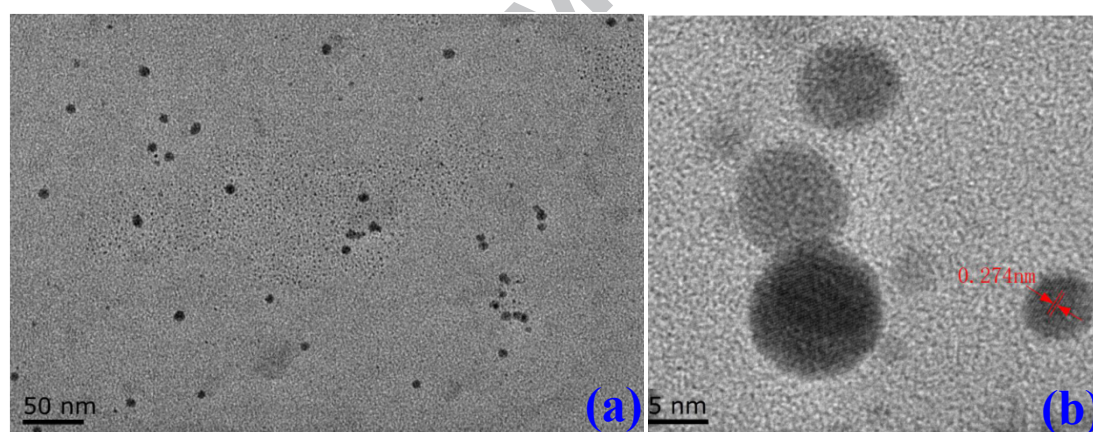


**Figure 3.** (a) TEM image of AgRh NPs; (b) HRTEM image of AgRh NPs.

The synthesis of GQDs-stabilized AgRh NPs **3-5** were conducted by using as-synthesized GQDs and sodium borohydride dissolved in water, and followed by the addition of different molar ratios of Ag and Rh salts(1:2, 1:1 and 2:1), respectively. Typically, the total amounts of AgNO<sub>3</sub> and Rh(NO<sub>3</sub>)<sub>3</sub> is fixed at  $2.5 \times 10^{-4}$  mmol. Ag (I) and Rh (III) ions were bonded to -COOH and -OH groups of the GQDs, and the corresponding nanoparticles have a small size and are good catalysts. However, the characteristic peaks of AgNPs do not appear in the UV-vis spectra of all the AgRh BNP **3-5**, due to the interference of RhNPs. **Figures 2 and 3** exhibit the representative TEM images of as-obtained AgRh BNPs with different Rh to Ag molar ratios. The monodispersed RhAg BNPs are homogeneously surrounded and stabilized by GQDs A. As the results of the NP

size distribution histogram, the sizes of AgRh BNPs **4** (4.52 nm) is much bigger than those of AgRh<sub>2</sub> BNPs **3** (2.10 nm) and Ag<sub>2</sub>Rh BNPs **5** (3.20 nm). Moreover, a representative HRTEM image of alloyed AgRh BNPs **4** also exhibits the (111) lattice fringe distance of 0.274 nm (**Figure 3b**), indicating an increase of the interatomic separation distance for alloyed AgRh BNPs.

The X-ray photoelectron spectroscopy (XPS) spectrum of **4** has also been recorded, for further verifying the exact oxidation states of the constituent metals in BNPs. The Rh 3d core level XPS spectrum of **4** is shown in **Figure 4a**. Rh 3d is fitted with two pair of peaks for the 3d<sub>5/2</sub> and 3d<sub>3/2</sub> doublets, the Rh 3d<sub>5/2</sub> and 3d<sub>3/2</sub> peak positions at 309.0 and 314.2 eV are assigned to Rh(0), respectively, whereas peaks at 310.3 and 315.3 eV correspond to 3d<sub>5/2</sub> and 3d<sub>3/2</sub> of Rh-O, respectively. It is clear that Rh has been partially oxidized to Rh<sub>2</sub>O<sub>3</sub>, due to the small size (4.52 nm) and the free molar energy of formation of Rh<sub>2</sub>O<sub>3</sub> (-39 kcal/mol). In fact, the excellent catalytic activity of Rh is crucially attributed to Rh<sub>2</sub>O<sub>3</sub> surface of RhNPs.<sup>[14]</sup> On the other hand, the Ag 3d<sub>5/2</sub> and Ag 3d<sub>3/2</sub> peaks at 368.2 and 374.1 eV, with a difference of 5.9 eV, is due to the Ag(0) in the **4** in **Figure 4b**, respectively. Thus, Rh has been partially oxidized to Rh<sub>2</sub>O<sub>3</sub> in the **4**, whereas the oxidation of Ag has not been observed.

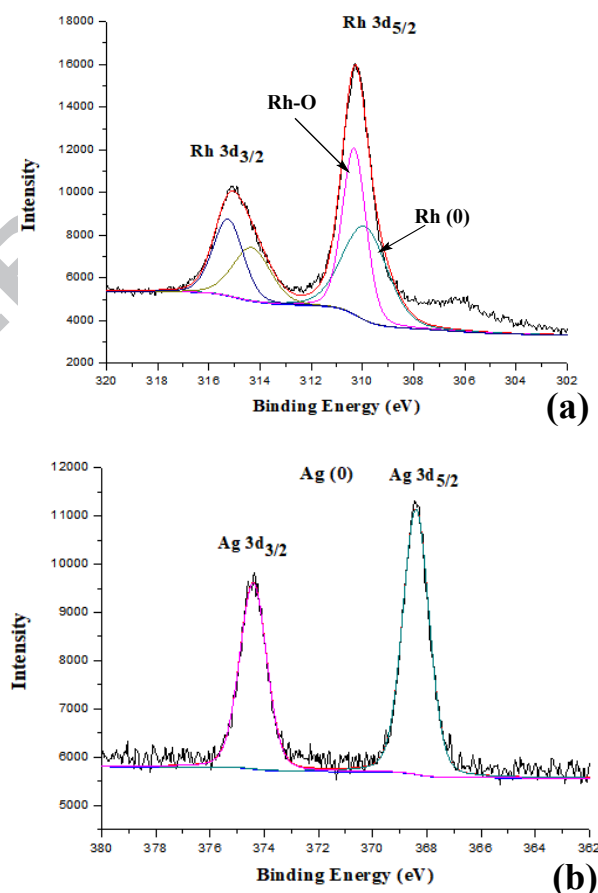
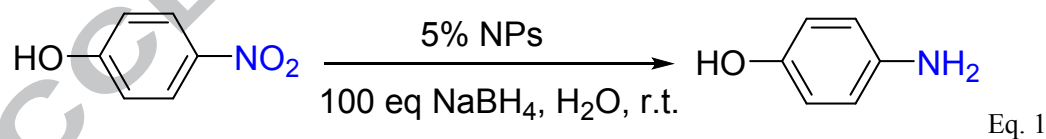


**Figure 4.** XPS spectra of (a) Rh 3d, and (b) Ag 3d over AgRh NPs.

### Compared catalytic performance of 1-5 in the 4-nitrophenol reduction by NaBH<sub>4</sub>

The catalytic performance of these AgRh BNPs have been investigated here in the reduction of 4-nitrophenol, a highly hazardous and poisonous pollutants, by sodium borohydride. The 4-nitrophenol reduction (eq. 1), which is a classic reaction for the assessment of the metal nanoparticles' catalytic properties, is easily monitored by UV-vis spectra due to the absorption band of 4-nitrophenol at 400 nm and that of 4-aminophenol at 300 nm, respectively.<sup>[15]</sup> The reduction of 4-nitrophenol has been carried out in the presence of 5.0 mol% NPs with 100 equiv of NaBH<sub>4</sub> in water at room temperature (Table 1 and Figure S6-S15 in the ESI). The results show all the reduction reaction did not need induction time (Table 1, entry 1-6). First, pure AgNPs 1 and RhNPs 2 are used in 5% mmol only providing  $k_{app}=2.0 \times 10^{-3}$  and  $2.8 \times 10^{-3} \text{ s}^{-1}$ , respectively (Table 1, entry 1 and 2). The reaction rate  $k_{app}$  of 4 ( $3.2 \times 10^{-3} \text{ s}^{-1}$ ) is much higher than these of 3 ( $2.5 \times 10^{-3} \text{ s}^{-1}$ ) and 5 ( $2.9 \times 10^{-3} \text{ s}^{-1}$ ) (Table 1, entry 3-5). It is obvious that 4 with molar ratio of 1:1 of Ag and Rh, shows the highest reaction rate among these BNPs (Table 1, entry 4), this is due to the positive synergistic effect of Ag and Rh atoms. In addition, to study the scope and generality of the present system, the reduction of 2,4-dinitrophenol (Eq. 2) and 4-nitrobenzene diazonium tetrafluoroborate (Eq. 3) have also been studied in the presence of 4 under the same condition as 4-nitrophenol reduction. The results exhibit that 2,4-dinitrophenol (the characteristic peaks at 360 nm and 440 nm decreases) and 4-nitrobenzene diazonium tetrafluoroborate (the characteristic peak at 400 nm decreases) have been successfully reduced to 2,4-diaminophenol and 4-aminobenzene diazonium niium tetrafluoroborate with the reaction rate  $k_{app}=2.0 \times 10^{-3}$  and  $1.4 \times 10^{-3} \text{ s}^{-1}$  (Figure S16- S19 in the ESI).

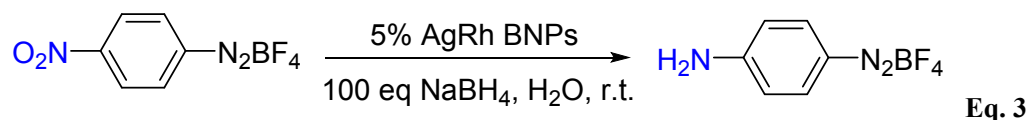
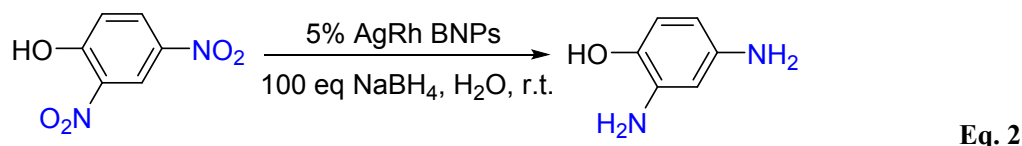
Table 1. 4-Nitrophenol reduction catalyzed by AgRh BNPs in water.<sup>a</sup>



Entry	TM ( $2.5 \times 10^{-4}$ mmol)	NPs	$T_0^b$ (s)	$K_{app}^c \times 10^{-3} \text{ s}^{-1}$	SPB <sup>d</sup> (nm)	D <sup>e</sup> (nm)
1	Ag	1	0	2	400	14.65
2	Rh	2	0	2.8	/	2.14
3	AgRh <sub>2</sub>	3	0	2.5	/	2.10
4	AgRh	4	0	3.2	/	4.52
5	Ag <sub>2</sub> Rh	5	0	2.9	/	3.20

<sup>a</sup>5.0 mol % NPs were used in the catalyzed 4-nitrophenol reduction NaBH<sub>4</sub> is in excess (100/1). <sup>b</sup>Induction time. <sup>c</sup>Rate constant.

<sup>d</sup>Surface plasmon band. <sup>e</sup>Core size (TEM) of the NPs.



#### Effect of AgRh BNPs 4-Generated Hydroxyl Radicals.

It is well-known that AgNPs have been demonstrated to catalyze conversion of  $\text{H}_2\text{O}_2$  into highly reactive oxidizing species such as hydroxyl radicals (Figure 5), via the Fenton-like reaction between AgNPs and  $\text{H}_2\text{O}_2$ .<sup>[16]</sup> The generation of hydroxyl radicals can be monitored by the system of  $\cdot\text{OH}$  oxidized reaction from methylene blue (MB) to MB-OH in the decrease of absorption of MB at 666 nm in the UV-vis spectrum. The time dependent UV-vis spectrum of MB during 0.05 mmol/L **4** and 0.25 mmol/L (5 eq)  $\text{H}_2\text{O}_2$  is shown in Figure 6a. After 25 mins, the peak of MB (666 nm) intensity decreases 0.170 is much higher than those of pure AgNPs (0.102) and pure RhNPs (0.032). It is expected that a drastic absorption change has been observed, verifying that generation of hydroxyl radicals induced by **4**, which is more efficient than pure AgNPs, and further oxidized MB to MB-OH. Then **4** induced  $\cdot\text{OH}$  generation has been studied with different concentration of hydrogen peroxide in Figure 6b (Figure S31-S36 in ESI). From 0.1 to 1.0 eq of  $\text{H}_2\text{O}_2$  (compared to the amount of **4**), the generation of hydroxyl radicals presents a linear relationship. While above 1 eq of  $\text{H}_2\text{O}_2$ , the production of hydroxyl radicals no longer increased, indicating the saturation of the reactivity of **4**. In addition, MB peak intensity remains unchanged without **4** or  $\text{H}_2\text{O}_2$ . It is completely consistent with the proposed Fenton-like reaction between AgNPs and  $\text{H}_2\text{O}_2$  for generating  $\cdot\text{OH}$ .

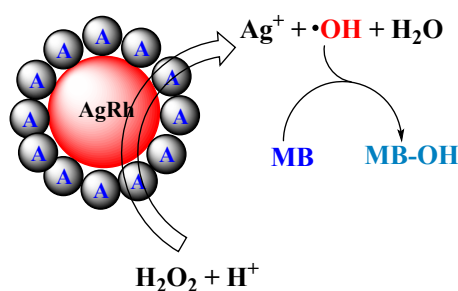
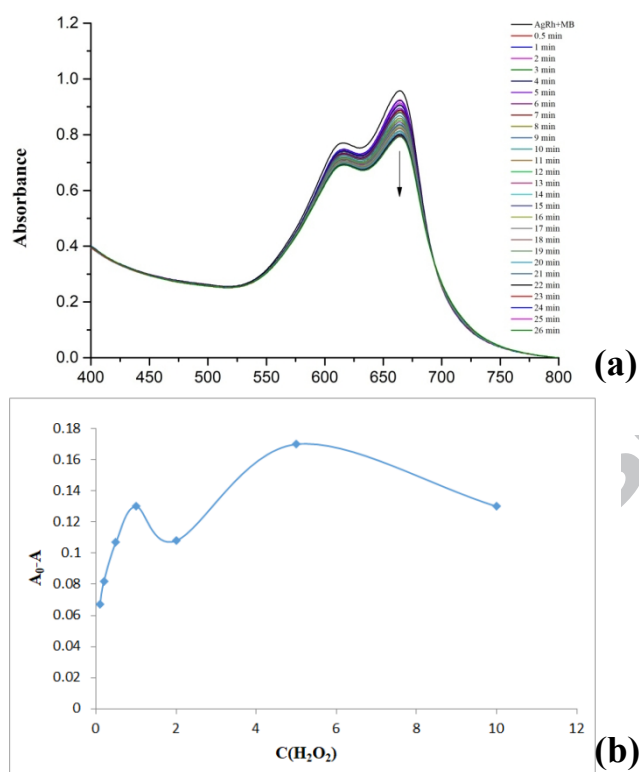


Figure 5. Schematic illustration of **4**-generated hydroxyl radicals.



**Figure 6.** (a) UV–Visible absorption spectra for the oxidation of methylene blue by **4** and 5 eq H<sub>2</sub>O<sub>2</sub>; (b) Effect of H<sub>2</sub>O<sub>2</sub> on the generation of hydroxyl radicals from samples containing 3 mL of  $1.5 \times 10^{-4}$  mmol **4**,  $3.375 \times 10^{-5}$  mmol methylene blue and H<sub>2</sub>O<sub>2</sub> at different concentrations.

### Conclusion

A green and facile method of synthesis of graphene quantum dots stabilized AgRh bimetallic nanoparticles has been developed in this work. Construction of pure AgNPs, pure RhNPs and AgRh BNPs **3-5** nanocomposites are accomplished by mixing GQDs and sodium borohydride, followed by the addition of simple commercial Ag or Rh salt at 0°C in water. Among them, **4** exhibits excellent catalytic performance in reduction of 4-nitrophenol by NaBH<sub>4</sub> and generation of hydroxyl radicals and further oxidized MB to MB-OH, via a positive synergistic effects between the Ag and Rh atoms on GQDs, than those of other BNPs and pure Ag or RhNPs. The present work provides a green and facile method for synthesis of high performance bimetallic NPs.

### Acknowledgment

Financial support from the National Natural Science Foundation of China (Grant No. 21805166),

the 111 Project of Hubei Province (Grant No. 2018-19-1) and China Three Gorges University is gratefully acknowledged.

## Reference

- [1] (a) Stamenkovic VR, Fowler B, Mun BS, Wang G, Ross PN, Lucas CA, Markovic NM (2007) Improved oxygen reduction activity on Pt<sub>3</sub>Ni(111) via increased surface site availability. *Science* 315(5811):493-497; (b) Tao F, Grass ME, Zhang Y, Butcher DR, Renzas JR, Liu Z, Chung JY, Mun BS, Salmeron M, Somorjai GA (2008) Reaction-driven restructuring of Rh-Pd and Pt-Pd core-shell nanoparticles. *Science* 322(5903):932-934; (c) Lim B, Jiang M, Camargo PHC, Cho EC, Tao J, Lu X, Zhu Y, Xia Y (2009) Pd-Pt bimetallic nanodendrites with high activity for oxygen reduction. *Science* 324(5932):1302-1305; (d) Omori T, Ando K, Okano M, Xu X, Tanaka Y, Ohnuma I, Kainuma R, Ishida K (2011) Superelastic effect in polycrystalline ferrous alloys. *Science* 333(6038): 68-71; (e) González E, Arbiol J, Puentes VF (2011) Carving at the nanoscale: sequential galvanic exchange and kirkendall growth at room temperature. *Science* 334(6061): 1377-1380.
- [2] (a) Liu X, Wang D, Li Y (2012) Synthesis and catalytic properties of bimetallic nanomaterials with various architectures. *Nano Today* 7(5):448-466; (b) Peng X, Pan Q, Rempel GL (2008) Bimetallic dendrimer-encapsulated nanoparticles as catalysts: a review of the research advances. *Chem Soc Rev* 37:1619-1628; (c) Gawande MB, Goswami A, Asefa T, Guo H, Biradar AV, Peng D, Zboril R, Varma RS (2015) Core-shell nanoparticles: synthesis and applications in catalysis and electrocatalysis. *Chem Soc Rev* 44:7540-7559; (d) Zhang L, Xie Z, Gong J (2016) Shape-controlled synthesis of Au-Pd bimetallic nanocrystals for catalytic applications. *Chem Soc Rev* 45:3916-3934; (e) Astruc D, Lu F, Ruiz J (2005) Nanoparticles as recyclable catalysts: the frontier between homogeneous and heterogeneous catalysis. *Angew Chem Int Ed* 44:7852-7872; (f) Liu X, Hamon JR, (2019) Recent developments in penta-, hexa- and heptadentate Schiff base ligands and their metal complexes. *Coord. Chem. Rev.* 389: 94-118; (g) Zhang HJ, Watanabe T, Okumura M, Haruta M, Toshima N (2012) Catalytically highly active top gold atom on palladium nanocluster. *Nat Mater* 11:49-52.
- [3] (a) Liu JH, Wang AQ, Chi YS, Lin HP, Mou CY (2005) Synergistic effect in an Au-Ag alloy nanocatalyst: CO Oxidation. *J Phys Chem B* 109(1):40-43; (b) Wang D, Villa A, Porta F, Prati L, Su D (2008) Bimetallic gold/palladium catalysts: Correlation between nanostructure and synergistic effects. *J Phys Chem C* 112(23):8617-8622; (c) Mott D, Luo J, Njoki PN, Lin Y, Wang L, Zhong CJ (2007) Synergistic activity of gold-platinum alloy nanoparticle catalysts. *Catal Today* 122(3-4):378-385; (d) Zhang L, Iyyamperumal R, Yancey DF, Crooks RM, Henkelman G (2013) Design of Pt-shell nanoparticles with alloy cores for the oxygen reduction reaction. *ACS Nano* 7(10):9168-9172.
- [4] Yayama T, Ishimoto T, Koyama M (2016) Theoretical investigation of hydrogen absorption properties of rhodium-silver alloys. *J. Alloy. Compd.* 662:404-408.
- [5] (a) Garcia S, Zhang L, Piburn GW, Henkelman G, Humphrey SM. (2014) Microwave synthesis of classically immiscible rhodium-silver and rhodium-gold alloy nanoparticles: Highly active hydrogenation catalysts. *ACS Nano* 8(11):11512-11521; (b) Wang C, Ciganda R, Yate L, Moya S, Salmon L, Ruiz J, Astruc D (2017) RhAg/rGO nanocatalyst: ligand-controlled synthesis and superior catalytic performances for the reduction of 4-nitrophenol. *J Mater Sci* 52 (16) : 9465-9476. (c) Roy A, Debnath B, Sahoo R, Chandrakumar KRS, Ray C, Jana J, Pal T (2016) Enhanced catalytic activity of Ag/Rh bimetallic nanomaterial: evidence of an ensemble effect. *J Phys Chem C* 120(10):5457-5467.
- [6] Inderwildi OR, Jenkins SJ, King DA (2007) When adding an unreactive metal enhances catalytic activity: NO<sub>x</sub> decomposition over silver-rhodium bimetallic surfaces. *Surface Science* 601 (17): L103-L108.

[7] (a) Hirakawa K, Toshima N (2003) Ag/Rh bimetallic nanoparticles formed by self-assembly from Ag and Rh monometallic nanoparticles in solution. *Chem Lett* 32(1):78–79; (b) Toshima N, Kanemaru M, Shiraishi Y, Koga Y (2005) Spontaneous formation of core/shell bimetallic nanoparticles: a calorimetric study. *J Phys Chem B* 109(34):16326–16331; (c) Yang A, Sakata O, Kusada K, Yayama T, Yoshikawa H, Ishimoto T, Koyama M, Kobayashi H, Kitagawa H (2014) The valence band structure of  $Ag_xRh_{1-x}$  alloy nanoparticles. *Appl Phys Lett* 105(15):153109; (d) Kusada K, Yamauchi M, Kobayashi H, Kitagawa H, Kubota Y (2010) Hydrogen-storage properties of solid-solution alloys of immiscible neighboring elements with Pd. *J Am Chem Soc* 132(45):15896–15898; (e) Dai Y, Wang Y, Liu B, Yang Y (2015) Metallic nanocatalysis: an accelerating seamless integration with nanotechnology. *Small* 11(3):268-289.

[8] (a) Li XM, Rui MC, Song JZ (2015) Carbon and graphene quantum dots for optoelectronic and energy devices: a review. *Adv Funct Mater* 25(31): 4929-4947. (b) Bacon M, Bradley SJ, Nann T (2014) Graphene quantum dots. *Part Part Syst Charact* 31(4): 415-428; (c) Li LS, Yan X (2010) Colloidal graphene quantum dots. *J Phys Chem Lett* 1(17): 2572-2576; (d) Tetsuka H, Asahi R, Nagoya A, Okamoto K, Tajima I, Ohta R, Okamoto A (2012) Optically tunable amino-functionalized graphene quantum dots. *Adv Mater* 24(39):5333-5338; (e) Suzuki N, Wang Y, Elvati P, Qu ZB, Kim K, Jiang S, Baumeister E, Lee J, Yeom B, Bahng JH, Lee J, Violi A, Kotov NA (2016) Chiral graphene quantum dots. *ACS Nano* 10(2):1744–1755; (f) Peng J, Gao W, Gupta BK, Liu Z, R-Aburto R, Ge L, Song L, Alemany LB, Zhan X, Gao G, Vithayathil SA, Kaiparettu BA, Marti AA, Hayashi T, Zhu JJ, Ajayan PM (2012) Graphene quantum dots derived from carbon fibers. *Nano Lett* 12(2):844-849; (g) Guo CX, Yang HB, Sheng ZM, Lu ZS, Song QL, Li CM (2010) Layered graphene/quantum dots for photovoltaic devices. *Angew Chem Int Ed* 49(17):3014-3017; (h) Ponomarenko LA, Schedin F, Katsnelson MI, Yang R, Hill EW, Novoselov KS, Geim AK (2008) Chaotic dirac billiard in graphene quantum dots. *Science* 320(5874): 356-358; (i) Liu F, Jang MH, Ha HD, Kim JH, Cho YH, Seo TS (2013) Facile synthetic method for pristine graphene quantum dots and graphene oxide quantum dots: origin of blue and green luminescence. *Adv Mater* 25(27):3657-3662; (j) Shen J, Zhu Y, Yang X, Li C (2012) Graphene quantum dots: emergent nanolights for bioimaging, sensors, catalysis and photovoltaic devices. *Chem Commun* 48: 3686-3699; (k) Yan X, Li Q, Li LS (2012) Formation and stabilization of palladium nanoparticles on colloidal graphene quantum dots. *J Am Chem Soc* 134(39):16095–16098.

[9] Ju J, Chen W (2015) In situ growth of surfactant-free gold nanoparticles on nitrogendoped graphene quantum dots for electrochemical detection of hydrogen peroxide in biological environments. *Anal Chem* 87(3):1903–1910.

[10] Shi J, Chan C, Pang Y, Ye W, Tian F, Lyu J, Zhang Y, Yang M, (2015) A fluorescence resonance energy transfer (FRET) biosensor based on graphene quantum dots (GQDs) and gold nanoparticles (AuNPs) for the detection of mecA gene sequence of staphylococcus aureus. *Biosens. Bioelectron.* 67:595-600.

[11] Niu X, Zhong Y, Chen R, Wang F, Liu Y, Luo D (2018) A “turn-on” fluorescence sensor for  $Pb^{2+}$  detection based on graphene quantum dots and gold nanoparticles. *Sensor. Actuat. B-Chem* 255 (2): 1577-1581

[12] (a) Liu X, Astruc D (2018) Atomically precise copper nanoclusters and their applications. *Coord. Chem Rev* 359:112-126; (b) Liu X, Astruc D (2017) From galvanic to anti-galvanic synthesis of bimetallic nanoparticles and applications in catalysis, sensing, and materials science. *Adv Mater* 29(16):1605305; (c) Liu X, Ruiz J, Astruc D (2017) Prevention of aerobic oxidation of copper nanoparticles by anti-galvanic alloying: gold versus silver. *Chem Commun* 53:11134-11137; (d) Liu X, Gregurec D, Irigoyen J, Martinez A, Moya S, Ciganda R, Hermange P, Ruiz J, Astruc D (2016) Precise localization of metal nanoparticles in dendrimer nanosnakes or inner periphery and consequences in catalysis. *Nat Commun* 7:13152; (e) Liu X, Ruiz J, Astruc D (2018) Compared catalytic efficiency of click-dendrimer-stabilized late transition metal nanoparticles in 4-nitrophenol reduction. *J Inorg Organomet Polym Mater* 28(2):399-406; (f) Astruc D, Deraedt C, Djeda R, Ornelas C, Liu X, Rapakousiou A, Ruiz J, Wang Y, Wang Q (2018) Dendromers, a family of super dendrimers with specific properties and

applications. *Molecules* 23(4):966;(g) Chen W, Shen J, Lv G, Li D, Hu Y, Zhou C, Liu X, Dai Z (2019) Green synthesis of graphene quantum dots from cotton cellulose. *ChemistrySelect* 4(10):2898-2902; (h) Yan J, Liu G, Li N, Zhang N, Liu X, (2019) Porphyrin-stabilized Transition Metal Nanoparticles and Their Applications in the Reduction of 4-Nitrophenol and Generation of Hydroxyl Radicals. *Eur. J. Inorg. Chem.* 23: 2806-2810; (i) Chen W, Shen J, Chen S, Yan J, Zhang N, Zheng K., Liu X, (2019) Synthesis of Graphene Quantum Dots Stabilized Gold Nanoparticles and Its Application, *RSC Adv.* 9:21215-21219.

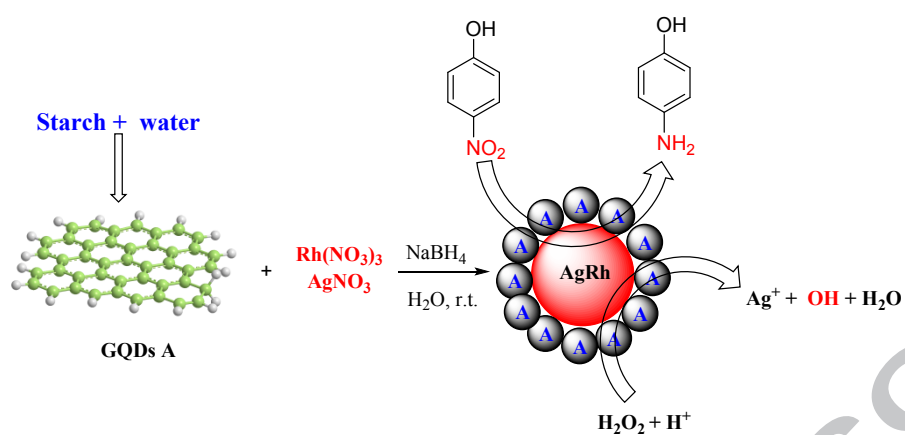
[13] Chen W, Li D, Tian L, Xiang W, Wang T, Hu W, Hu Y, Chen S, Chen J, Dai Z (2018) Synthesis of graphene quantum dots from natural polymer starch for cell imaging. *Green Chem* 20:4438-4442.

[14] (a) Kim SM, Qadir K, Seo B, Jeong HY, Joo SH, Terasaki O, Park JY (2013) Nature of Rh oxide on Rh nanoparticles and its effect on the catalytic activity of CO oxidation. *Catal Lett* 143:1153-1161; (b) Kim S, Qadir K, Jin S, Reddy AS, Seo B, Mun BS, Joo SH, Park JY (2012) Trend of catalytic activity of CO oxidation on Rh and Ru nanoparticles: role of surface oxide. *Catal Today* 185:131-137

[15] (a) Kuroda K, Ishida T, Haruta M (2009) Reduction of 4-nitrophenol to 4-aminophenol over Au nanoparticles deposited on PMMA. *J Mol Catal A: Chem* 298(1-2):7-11; (b) Wunder S, Polzer F, Lu Y, Ballauff M (2010) Kinetic analysis of catalytic reduction of 4-nitrophenol by metallic nanoparticles immobilized in spherical polyelectrolyte brushes. *J Phys Chem C* 114(19):8814-8820; (c) Saha S, Pal A, Kundu S, Basu S, Pal T (2010) Photochemical green synthesis of calcium-alginate-stabilized Ag and Au nanoparticles and their catalytic application to 4-nitrophenol reduction. *Langmuir* 26(4):2885-2893; (d) Wang SN, Zhang MC, Zhang WQ (2011) Yolk-shell catalyst of single Au nanoparticle encapsulated within hollow mesoporous silica microspheres. *ACS Catal.* 1(3):207-211; (e) Wunder S, Lu Y, Albrecht M, Ballauff M (2011) Catalytic activity of faceted gold nanoparticles studied by a model reaction: evidence for substrate-induced surface restructuring. *ACS Catal* 1(8):908-916; (f) Li J, Liu CY, Liu Y (2012) Au/graphene hydrogel: synthesis, characterization and its use for catalytic reduction of 4-nitrophenol. *J Mater Chem* 22:8426-8430; (g) Liu FF, Liu X, Astruc D, Gu HB, (2019) Dendronized triazolyl-containing ferrocenyl polymers as stabilizers of gold nanoparticles for recyclable two-phase reduction of 4-nitrophenol. *J. Colloid. Interf. Sci.* 533:161-170; (h) Liu X, Mu SD, Long YR, Qiu, GR, Ling, Q J, Gu HB, Lin W, (2019) Gold Nanoparticles Stabilized by 1,2,3-Triazolyl Dendronized Polymers as Highly Efficient Nanoreactors for the Reduction of 4-Nitrophenol. *Catalysis Letters*, 149 (2):544-551; (i) Liu Y, Mu SD, Liu X, Ling QJ, Hang, CD, Ruiz J, Astruc D, Gu HB, (2018) Ferrocenyl Janus mixed-dendron stars and their stabilization of Au and Ag nanoparticles. *Tetrahedron*, 74(37):4777-4789; (j) Zhao L, Ling Q, Liu X, Hang C, Zhao Q, Liu F, Gu HB, (2018) Multifunctional triazolylferrocenyl Janus dendron: Nanoparticle stabilizer, smart drug carrier and supramolecular nanoreactor. *Appl. Organomet. Chem.*, 32(2): e4000.

[16] (a) Wang L, Zheng J, Li Y, Yang S, Liu C, Xiao Y, Li J, Cao Z and Yang R (2014) AgNP-DNA@GQDs hybrid: new approach for sensitive detection of H<sub>2</sub>O<sub>2</sub> and glucose via simultaneous AgNP etching and DNA cleavage. *Anal Chem* 86(24):12348-12354. (b) He W, Zhou YT, Wamer WG, Boudreau MD, YinJJ (2012) Mechanisms of the pH dependent generation of hydroxyl radicals and oxygen induced by Ag nanoparticles. *Biomaterials* 33(30):7547-7555; (c) Mohamed RM, Aazam ES (2014) Novel Ag/YVO<sub>4</sub> nanoparticles prepared by a hydrothermal method for photocatalytic degradation of methylene-blue dye. *J Ind Eng Chem* 20(6): 4377-4381.

1. The design and synthesis of highly efficient and ultrafine bimetallic nanoparticles catalysts is challenging.
2. Here we report the synthesis of AgRh bimetallic nanoparticles stabilized by graphene quantum dots (GQDs)
3. Their exceptional catalytic activities in the reduction of 4-nitrophenol, 2,4-dinitrophenol and 4-nitrobenzene diazonium tetrafluoroborate and generation of hydroxyl radicals.



The design and synthesis of highly efficient and ultrafine bimetallic nanoparticles catalysts is challenging. Here we report synthesis of graphene quantum dots-stabilized bimetallic AgRh nanoparticles and their exceptional catalytic activity in the reduction of 4-nitrophenol, 2,4-dinitrophenol and 4-nitrobenzene diazonium tetrafluoroborate and generation of hydroxyl radicals.